ELSEVIER

Wear 253 (2002) 1145–1155

WEAR

www.elsevier.com/locate/wear

Nanotribology of CoCr–UHMWPE TJR prosthesis using atomic force microscopy

Sunita P. Ho [c], Robert W. Carpick [b], Thomas Boland [a], Martine LaBerge [a,*]

[a] *Department of Bioengineering, 501 Rhodes Engineering Research Center, Clemson University, Clemson, SC 29634-0905, USA*
[b] *Department of Engineering Physics, University of Wisconsin at Madison, 1500 Engineering Dr., Madison, WI 53706-1687, USA*
[c] *Department of Preventive and Restorative Dental Sciences, Division of Biomaterials and Bioengineering, University of California San Francisco, 707 Parnassus Avenue, San Francisco, CA 94143-0758, USA*

Received 24 September 2001; received in revised form 17 July 2002; accepted 17 July 2002

Abstract

Ultra high molecular weight polyethylene (UHMWPE) submicron wear debris particles in total joint replacement (TJR) prosthesis have been observed clinically to cause osteolysis. In this study, the formation of UHMWPE submicron wear debris was investigated by modeling a nanoscale asperity on the surface of a CoCr femoral component of a total knee replacement (TKR) prosthesis using a Si_3N_4 AFM commercial tip. Contact mode atomic force microscope (AFM) was used as a tribosystem to represent CoCr–UHMWPE asperity contact in TKR prostheses in order to evaluate nanoscale coefficient of friction 'μ'. Nanoindentation was used to understand the mechanical response of the TJR prosthesis components. Moreover, the threshold for UHMWPE plastic deformation and subsequently wear as a function of frictional and normal load at a nanoscale between CoCr alloy and UHMWPE asperity-to-asperity contact was investigated.

Results from energy dispersive X-ray (EDX) analysis and back scattering energy (BSE) technique illustrated the presence of silicon carbide (SiC) particles in the polished surface of a femoral component of total knee replacement (TKR) prosthesis. Sliding of the model asperity on direct compression moulded UHMWPE for a total normal load range of 1–11 nN caused contact pressures ranging from 14 to 80 MPa which resulted in the dynamic 'μ' at the interface of the nanotribocontact equal to 0.22 ± 0.01. Transients in frictional response of the UHMWPE as a function of normal load range (17–340 nN) during sliding against the modeled CoCr asperity were observed. The first transient in frictional force was observed at a normal load of 197 ± 9 nN, corresponding to a contact pressure of 462 ± 9 MPa. The second transient in the frictional force was observed at a normal load of 288 ± 13 nN corresponding to a contact pressure of 518 ± 13 MPa. Following the second transition in frictional response for the normal load range selected, plowing of the UHMWPE surface by the hard asperity was observed. This indicated that the deep scratches noticed in retrieved TJR prosthesis could be due to the abrasion from protruding hard carbide asperities that exist within the cast CoCr alloy of TJR prosthesis. From this study it can be stated that the plastic deformation of UHMWPE under multiaxial loading conditions (normal and shear) during sliding can be used to explain the initiation of failure of the UHMWPE insert in TJR prosthesis eventually leading to submicron wear debris generation.

Keywords: Friction transient; Atomic force microscopy (AFM); Ultra high molecular weight polyethylene (UHMWPE); Cobalt chromium (CoCr)

1. Introduction

Total joint replacement (TJR) prostheses consist of metallic and non-metallic components (mirror-finish cast cobalt chromium alloy or stainless steel or ceramic articulating on a metallic, ceramic or a polymeric ultra high molecular weight polyethylene (UHMWPE) counter components) [1,2]. In particular, CoCr alloy femoral components are used in TJR prostheses because of their excellent wear resistance. It has been suggested that CoCr alloys with higher carbon composition may possess superior wear resistance due to the size and disposition of the carbides within the alloy, and particularly at the polished-bearing surface [3].

Since 1962, UHMWPE has been the principal material used to replace damaged cartilage in total joint arthroplasties [1,2,4]. The very long molecular chain structure of UHMWPE results in extensive mechanical entanglements of the molecular chains, imparting relatively higher abrasion resistance compared to other polymeric-bearing biomaterials [5]. Additionally, abrasive resistance of polymeric-bearing surface can be increased by radiation cross-linking of the UHMWPE molecular chains [6].

Despite the many advantages of UHMWPE and its widespread use for mechanical engineering applications [1,2,4,5], the generation of UHMWPE submicron wear

* Corresponding author. Tel.: +1-864-656-5557; fax: +1-864-656-4466.
E-mail address: laberge@ces.clemson.edu (M. LaBerge).

0043-1648/02/$ – see front matter © 2002 Elsevier Science B.V. All rights reserved.
PII: S0043-1648(02)00220-X

debris, also termed as nanoscale wear debris, in TJR prostheses has been of primary concern [7,8]. The submicron polyethylene wear particles have been observed clinically to cause an inflammatory reaction leading to bone resorption (osteolysis) and device failure [3,8]. As particles accumulate in periprosthetic tissues, the cellular response may include the release of biochemical substances believed to be responsible for the development of cystic lesions that may lead to the loss of fixation of the device [8].

Over the past 4 decades, the school of thought for the submicron wear debris generation considering material related factors has been divided primarily into two major sources: (1) classical adhesive, abrasive and third-body wear processes occurring in vivo; and (2) release of particles that are inherent to the microstructure of UHMWPE. The first paradigm of submicron wear debris generation was studied from purely a mechanistic approach. The combined effort of in vitro joint simulation [9], finite element modeling and numerical modeling studies [10], elucidated the cause of different wear mechanisms in UHMWPE at a macroscopic scale defining the failure of the UHMWPE insert in TJR prosthesis. These studies attempted to define the cause of submicron wear debris by addressing the accumulation of large amounts of plastic strain. It was suggested that large-scale deformations, texture evolution, fracture and surface rupture within the surface region of UHMWPE components over repeated cyclic motion could cause macroscopic failure in the material eventually leading to total failure of the implant [7]. Although these studies provide insight to wear processes in TJR prostheses, they do not explain the initiating cause of the submicron wear debris generation.

The second paradigm of submicron wear debris generation was studied from purely a materials approach. A microscopic examination of the morphology of retrieved UHMWPE wear debris nanostructure was compared with the morphology of virgin UHMWPE powder nanostructure, and the morphology of sectioned samples fabricated from virgin UHMWPE powder. Despite the many possible sources of submicron wear debris considered in these studies, the initiating cause of origination of UHMWPE wear debris particles in TJR prosthesis was not addressed [11,12].

Currently, there is a transition from continuum macroscale to consideration of discrete asperity-to-asperity nanoscale contact [13]. This may provide insight into the production of submicron wear debris, which eventually leads to failure of the UHMWPE surface of TJR prosthesis. During sliding between the two contacting surfaces of a TJR prosthesis, multiple asperity contacts, adhesion-induced deformation, and plowing of the surfaces by wear particles or hard asperities on the counter surface occur at the solid–solid interface. It is well documented that when two engineering surfaces come into contact, plastic deformation may occur at the tips of asperities within the softer material [14,15]. The wear performance of the relatively soft UHMWPE polymeric material would be influenced by the surface characteristics of its hard, cast CoCr metal counterpart (Table 1). Moreover, despite the prevailing modes of fluid and boundary lubrication, a partial dry intimate asperity-to-asperity contact in TJR prosthesis can be established [9].

Table 1
Comparison of mechanical properties of silicon carbide, silicon nitride, cast CoCr alloy and UHMWPE

Material	Modulus (GPa)	Hardness (MPa)
Silicon carbide (SiC) [30]	440	245
Silicon nitride (Si_3N_4) [30]	310	204
Cast cobalt chromium (CoCr)[a]	275 ± 11.5	6.2 ± 0.5
Ultra high molecular weight polyethylene (UHMWPE)[a]	2.29 ± 0.1	0.07 ± 0.01

[a] Measured using a nanoindenter at a penetration depth of 500 nm (MTS-Nanoinstruments, TN, USA).

Nanometer scale asperity contacts are essential elements in microscopic models of macroscopic contacts as formulated earlier by Bowden and Tabor [14]. In each of these areas, it is essential to understand the frictional response of these contacts, particularly under combined normal and resulting shear loading at the interface of the various tribosystems. Over the past decade, the damage thresholds for materials like mica, alkali halides, low density and high density polyethylene were defined using AFM by measuring lateral force as a function of normal load [16–18].

Additionally, AFM was used to model plowing wear mechanisms to help understand the scratch resistance of UHMWPE and subsequently the generation of nanoscale wear debris particles in TJR prosthesis [19,20]. However, none of these studies addressed the damage threshold and the result of plastic deformation of UHMWPE associated to surface wear. In order to explain the plastic strain accumulation, the assumptions of onset of plasticity have yet to be explored for UHMWPE in the context of TJR prosthesis [21].

In this study, it was considered that the initial load-bearing area in a total joint prosthesis is distributed over many of the nanometer scale asperity-to-asperity contacts. Hence, the deformation and controlled wear process of direct compression moulded UHMWPE articulating against cast CoCr alloy of TJR prosthesis was studied by modeling an intimate asperity-to-asperity contact between the two articulating surfaces of TJR prosthesis using atomic force microscopy (AFM). In addition, the precursors to the formation of polymeric wear debris of a compression moulded UHMWPE tibial insert were determined.

In this study, initially, the surface topography of surgical grade femoral and tibial components in a total knee replacement (TKR) prosthesis were studied in addition to the frictional response of UHMWPE within and beyond its elastic regime when in contact with a nanoasperity on the femoral component surface. Additionally, it was hypothesized that the primary energy dissipation process (frictional work) of UHMWPE is gross plastic deformation leading to plowing during the asperity-to-asperity nanocontact of a cast CoCr femoral component articulating against a direct compression moulded UHMWPE insert. The threshold for plastic

deformation and subsequently wear as a function of frictional and normal load at a nanoscale between CoCr alloy and UHMWPE asperity-to-asperity contact was also determined thereby defining the precursors to the formation of polymeric wear debris.

2. Materials and methods

2.1. Surgical grade CoCr alloy femoral component and UHMWPE sample preparation procedure

Packaged surgical grade commercial cast cobalt chromium (CoCr) alloy (Maxim^{TM}, Biomet INC., IN, USA) femoral component was sectioned into 5 mm × 5 mm × 10 mm samples using a 420si wire electric discharge machine (EDM) (Spirit Machinery Inc., NY, USA). A γ-sterilized and packaged surgical grade commercial direct compression moulded UHMWPE tibial insert manufactured from Himont 1900 powder (Maxim^{TM}, Biomet INC., IN, USA) was sectioned to 7 mm × 7 mm × 5 mm samples using a band saw (Delta International Machinery Corp., PA, USA). The samples were ultrasonicated for 10 min in 1% liquinox^{TM} solution [22] (ALCONOX Inc., NY, USA) followed by 40 min sonication in deionized water. The samples were then sonicated for an additional 40 min in 99.9% pure acetone (Aldrich, WI, USA) and placed in a dessicator at room temperature until used. The above stated cleaning protocol was used in order to avoid the influence of contaminants such as grease when scanning the samples using an AFM. Hence, the tibial insert was initially cleaned with an anionic liquid detergent (liquinox^{TM}) followed by removal of the contaminants with deionized water. The final agent acetone facilitated in removing the left over water molecules from the surface of the tibial insert [23]. The integrity of the bearing surface of the tibial insert and the prepared samples was preserved at all times during cleaning.

The relative difference in roughness between UHMWPE and CoCr alloy samples was determined by evaluating the respective surface's roughness average 'R_a'. The 'R_a' and radius of curvature of asperities on areas ranging from 5 μm × 5 μm to 25 μm × 25 μm on UHMWPE and CoCr alloy samples was evaluated using an atomic force microscope (AFM). A commercially available silicon nitride (Si_3N_4) square pyramidal tip attached to a 'D'-type, 'V'-shaped cantilever with a nominal spring constant of 0.03 N/m (MSCT-AUNM, ThermoMicroscopes, CA, USA) was used. The areas were scanned at a frequency of 2.0 Hz using a 175 μm × 175 μm piezo with ambient air as medium at a temperature of 22 °C. Physiologically relevant medium was not used in this study in order to eliminate the influence of various macromolecules within the medium at the nanoscale contact of the AFM tip and sample surface.

Qualitative topographical analysis of areas ranging approximately from 25 μm × 20 μm to 600 μm × 400 μm of polished surface of cast CoCr alloy was performed using scanning electron microscopy (SEM) (S-3500H, Hitachi Scientific Instruments, Japan) techniques with an electron beam energy of 15 keV. The elemental composition and location of the elements of cast CoCr alloy samples were investigated using energy dispersive X-ray (EDX) analysis and back scattering energy (BSE) technique.

2.2. Determination of nanomechanical properties of CoCr alloy and UHMWPE

A nanoindentation feasibility study (MTS-Nanoinstruments, TN, USA) was performed on CoCr alloy and UHMWPE samples by mounting the respective samples (CoCr alloy and UHMWPE) on two individual aluminum stubs using cyanoacrylate adhesive (Permatex Brands & Technologies Inc., OH, USA). The indenter used for nanomechanical property evaluation was a Berkovich diamond indenter [24]. Before nanoindenting the sample surfaces, 6061 aluminum was indented and the impressions inspected with an optical microscope to ensure that the Berkovich tip was clean. Indenter tip calibration was verified by indenting in fused silica. The constant displacement rate method was used to evaluate the nanomechanical properties of the sectioned sample [25]. Each sample had a maximum of 10 indents at a penetration depth of 500 nm. Hardness and compression modulus were calculated as an average of the 10 indents (Table 1).

2.3. Determination of nanoscale coefficient of friction, contact area and contact pressure of TJR prosthesis

The frictional force microscopy (FFM) mode was used to evaluate frictional load as a function of external applied normal load [26] and to determine the coefficient of friction 'μ' at a nanoscale of an asperity-to-asperity contact of TJR prosthesis. The 'μ' of direct compression moulded UHMWPE sliding against the Si_3N_4 AFM tip was obtained by loading the contact within the elastic limit of the compression moulded UHMWPE (Tables 1 and 2). The frictional load as a function of normal load in this study was acquired for every 5% decrease in normal load by scanning the tip repeatedly over a 1 μm line on the UHMWPE tibial surface. This was accomplished by disabling the slow scan axis of the AFM piezo. The frictional and normal loads were recorded until the tip retracted from the sample surface offering zero frictional resistance. A scanning frequency of 2 Hz, which is considerably lower than the frequency observed during a normal gait cycle, was used when recording the frictional load. Based on pilot studies performed no significant change in the frictional behavior was observed for higher scanning frequencies over a scan length of 1 mm. Moreover, scanning the sample at higher frequencies introduced extraneous noise into the recorded data, a characteristic of AFM. Hence, a suitable frequency of 2 Hz was used when scanning the UHMWPE sample using a cantilever with a nominal spring constant of 0.03 N/m.

Table 2
Experimental parameters used to study friction coefficient and wear characteristics of a nanotribological contact in TJR prosthesis

Parameter (units)	FFM using a cantilever with a spring constant of	
	0.028 ± 0.003 N/m	2.1 N/m
Cantilever	'D'-type, 'V'-shaped ultralever	'D'-type, 'V'-shaped microlever
Radius of curvature (nm)	40	45
Total normal load 'N' (N)	1–11	17–340
Contact area 'A' (m^2)	5×10^{-17} to 1×10^{-16}	9×10^{-17} to 6×10^{-16}
Contact pressure 'P' (MPa)	14–80	209–552
Friction coefficient 'μ'	0.22 ± 0.01	–

The 'μ' was calculated by converting the electric signals of normal load 'N_v' and resulting frictional load 'F_v' from volts 'V' to corresponding units of force in Newtons 'N'. The normal load and frictional load on the sample were determined by evaluating the normal spring constant 'k_N' and the proportionality constant 'ζ' for a 'V'-shaped, 'D'-type cantilever. The proportionality constant for lateral load conversion was determined by using the 'wedge method' and $SrTiO_3$ crystal with well-defined tilted planes of (1 0 1) and (1 0 3) mesoscale $SrTiO_3$ crystal (WiTEC, Ulm, Germany) [26].

Normal spring constant of the cantilever was evaluated based on thermal fluctuations of the cantilever despite its limitations like other existing methods [27]. The radius of curvature of the tip before and after frictional load measurement was studied using the $SrTiO_3$ crystal. Since the produced traces were images of the scanning tip, the tip radius of curvature was found by fitting a parabola to the apex of each section plot of the topography image. The following equation was implemented in evaluating 'μ' at the modeled nanocontact of TJR prosthesis:

$$\mu = \frac{F_v \times \zeta}{N_v \times k \times k_N \times 10^{-9}} \quad (1)$$

The contact area was determined in terms of the tip radius, applied normal load, adhesive forces and elastic properties of the surfaces using Johnson–Kendall–Roberts (JKR) theory [28]. The elastic modulus of UHMWPE and Si_4N_3 are shown in Table 1. A Poisson's ratio of 0.3 was assumed for Si_4N_3 and 0.45 for UHMWPE. The contact pressure was determined by dividing the normal load with the contact area calculated (Table 2).

2.4. Onset of plastic deformation at a nanometer scale using AFM as a tribosystem

The response of UHMWPE at higher normal loads was studied using a Si_3N_4 AFM tip attached to a 'V'-shaped, 'A'-type ultralever (ULNC-AUNM, ThermoMicroscopes, CA, USA) with a nominal normal spring constant of 2.1 N/m. The procedure for acquiring frictional response of UHMWPE as a function of normal load was identical to that stated when loading the contact within the elastic regime of UHMWPE (Tables 1 and 2). Initially, no contact was allowed between the two-modeled nanoscale surfaces in order to prevent any irreversible deformation of the polymeric surface due to the high normal stiffness of the cantilever. After the contact between the two surfaces was established, the frictional resistance offered by the UHMWPE surface was recorded for every 5% increase in normal load. The normal load was increased in an attempt to understand the contribution of plastic and gross deformation of the polymeric surface due to multiaxial loading (normal and frictional resistance) at the modeled contact.

The data obtained from the friction test using a cantilever with a nominal spring constant of 2.1 N/m was divided into reversible UHMWPE deformation and irreversible UHMWPE damage. The contact area and contact pressure for reversible UHMWPE deformation was determined similar to that described in Section 2.3. The contact area and pressure for the irreversible region was determined by dividing the normal load by the projected contact area obtained from tip geometry and measured wear track depth [17].

A scanning frequency of 2 Hz was used to perform the friction test. In addition to the reasons stated in Section 2.3, the use of 2 Hz as scanning frequency facilitated in observing the abrupt changes in friction at the contact of the AFM tip and the UHMWPE sample when using a cantilever with a spring constant of 2.1 N/m.

At higher normal loads, a piece-wise linear regression model was used to understand the occurrence of transitions in frictional load determined at some value of normal load 'N_{vi}' defined as the point of discontinuity [29]. The 'N_{vi}' value chosen by iterations was that which provided the minimum sum of squares error. The linear regression model used to determine the validity of the sudden transitions in the frictional measurement, as a function of normal load was as follows (Fig. 1):

$$Y = \alpha_0 + \alpha_1 \times X_1 + (\alpha_1 - \beta_1) \times (N_{vi} - X_1) \times X_2 + X_2 \times \delta \quad (2)$$

where, N_{vi} is the point where transition in frictional load occurred; δ the shift, if any, between the two linear lines; α_0 the intercept for linear regression line 1; α_1 the slope for linear regression line 1; β_0 the intercept for linear regression line 2; β_1 the slope for linear regression line 2. SAS V8.0 was used to solve and define the values of the individual

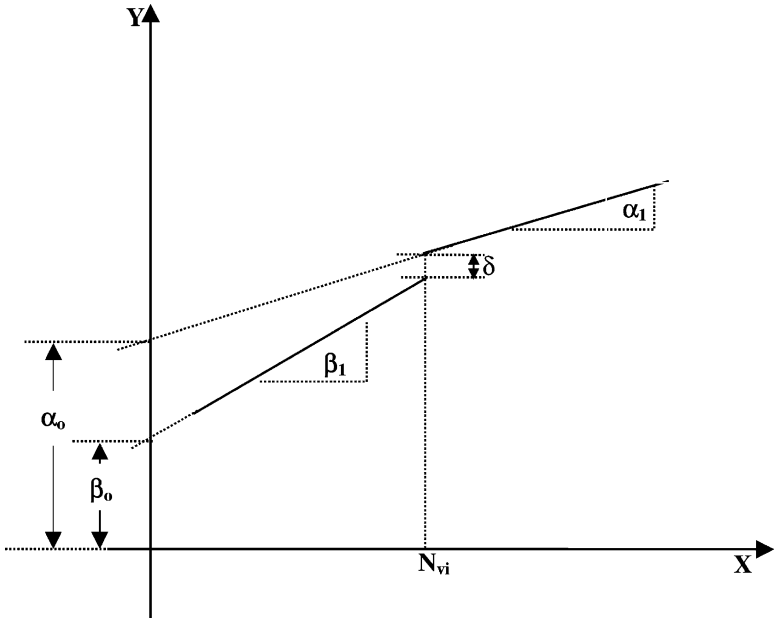

Fig. 1. Piece-wise linear regression model [29].

parameters in the linear regression model (SAS Institute Inc., NC, USA).

3. Results

The geometry and elemental composition of the asperities on the CoCr femoral component was compared to the geometry and elemental composition of the AFM tip. SEM micrographs of CoCr femoral component revealed scratches, cast imperfections and micrometer asperities and pits on the mirror like polished surface of CoCr alloy femoral component surface (Fig. 2). AFM topographical scans of cast CoCr surface also showed craters, pits, peaks and scratches (Fig. 3). In any given SEM micrograph, the darker regions corresponded to low atomic weight elements and the lighter regions corresponded to high atomic weight elements. EDX along with spot analysis on each contrasting image corresponded to a single element as shown in the back scattering energy micrographs (Fig. 2). The black regions corresponded to silicon carbide (SiC) while the dark gray regions were chromium carbide (CrC), and any other region besides black and dark gray was predominantly an alloy of Co and Cr (Fig. 2). The range of the maximum width of the silicon carbide asperities was approximately 2–10 μm and the range of maximum width of the chromium carbide asperities was approximately 2–5 μm. Although the modulus of elasticity of Si_3N_4 is less than the modulus of SiC, but of the same order of magnitude, the hardness of the two materials is approximately the same (Table 1). The 'R_a' determined using AFM for four different regions on the same sample surface of the femoral component are shown in Table 3. Section analysis on the AFM topography scans revealed a range of radii of curvature 25–75 nm of the nanoscale asperities of cast CoCr femoral component. The radii of curvature of commercially available Si_3N_4 tips typically ranges from 10 to 100 nm [18]. This similarity in asperity size demonstrates the validity of using the AFM tip as a model asperity. The measured radius of curvature of Si_3N_4 tip, using the $SrTiO_3$ crystal used in this study was approximately 40 nm [26].

Areas of surgical grade γ-sterilized direct compression moulded UHMWPE samples ranging from 5 μm × 5 μm to 25 μm × 25 μm revealed scratches and mould imperfections and micrometer asperities on the UHMWPE surface (Fig. 4). The 'R_a' parameters evaluated at four different regions for each of the three scan areas on the same sample surface of the UHMWPE insert are shown in Table 3. A Student's *t*-test with a significance level of 0.05, revealed a significant difference in 'R_a' between cast CoCr and compression moulded UHMWPE at each individual scan area (Table 3). The 'R_a' of the CoCr femoral component surface was significantly higher than the UHMWPE tibial component surface over the scanned area range of 5 μm × 5 μm to 25 μm × 25 μm (Table 3).

The normal spring constant of the 'D'-type, 'V'-shaped cantilever measured using thermal fluctuation method was

Table 3
Roughness average 'R_a' ($n = 4$) for cast CoCr alloy and direct compression moulded UHMWPE

Scanned area (μm^2)	'R_a' cast CoCr alloy (nm)	'R_a' direct compression moulded UHMWPE (nm)	*P* value[a]
625.0	31.1 ± 4.2	15.3 ± 1.6	0.0018
100.0	26.6 ± 5.5	12.6 ± 7.3	0.0007
25.00	20.9 ± 6.9	9.05 ± 3.9	0.0004

[a] Significance level = 0.05.

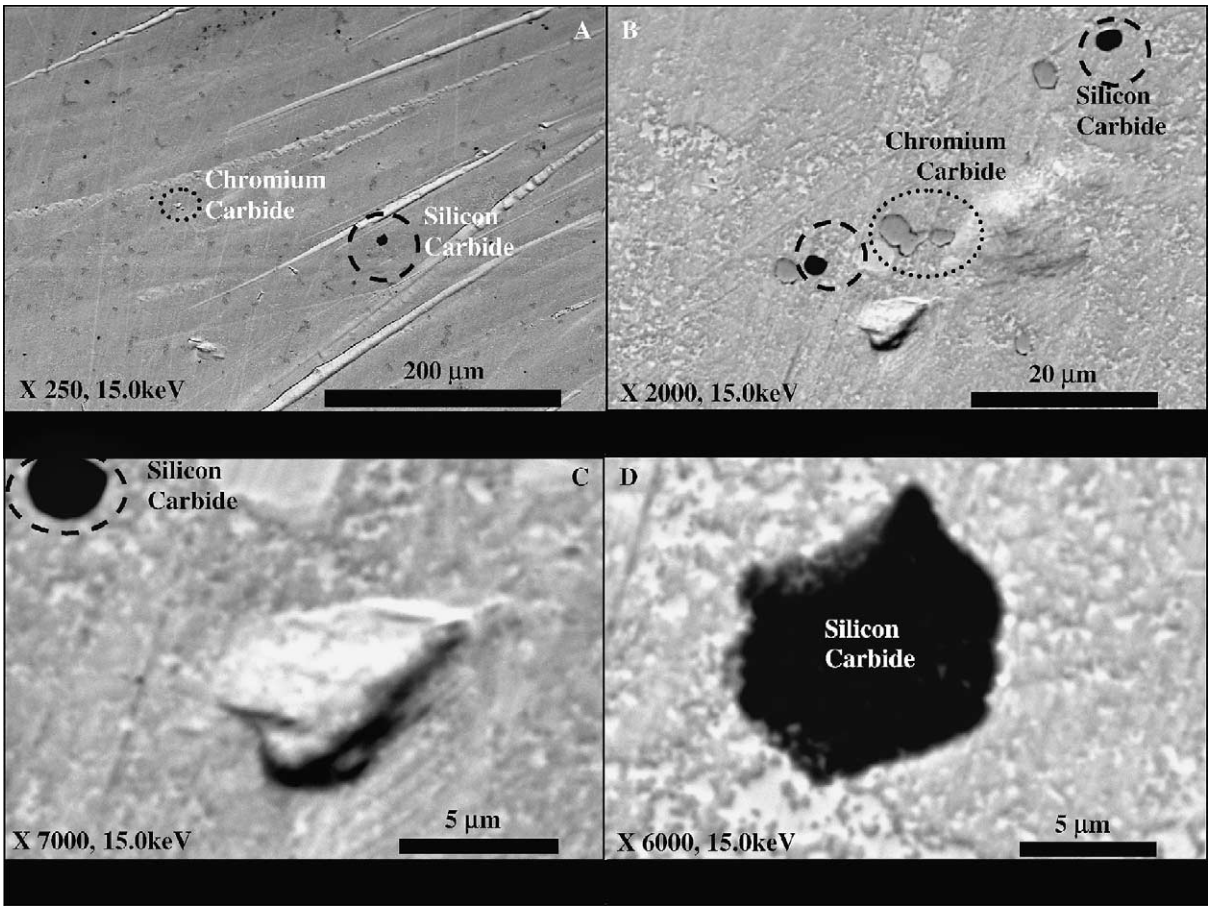

Fig. 2. Scanning electron microscopy (SEM) micrographs (15 keV, at different magnifications: A, B, C, D) of cast cobalt chromium alloy. The contrasting image of white, grey, black was obtained using back scattering energy technique (BSE). Black spots—silicon carbides (notice several regions of silicon carbide on the polished cast cobalt chromium surface); grey spots—chromium carbide; and any other region—an alloy of chromium and cobalt. The cast imperfections, microasperities, pits and scratches, regions of chromium exclusively and several regions of silicon carbide embedded from the polishing grit of silicon carbide can be noticed.

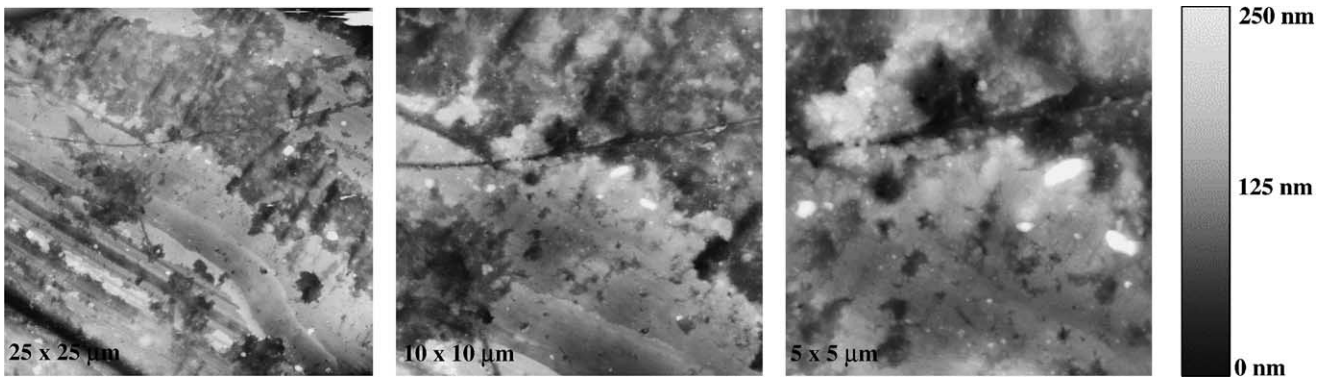

Fig. 3. Atomic force microscopy scans of cast CoCr alloy femoral component of (Maxim^{TM}, Biomet Inc., IN, USA) total knee replacement prosthesis. The surfaces were scanned using a silicon nitride AFM tip, 'V'-shaped, 'D'-type microlever with a normal spring constant of 0.028 ± 0.003 N/m (ThermoMicroscopes, CA, USA).

0.028 ± 0.003 N/m. The constant multiplication factor 'ζ' for frictional force unit conversion was equal to 43.19 ± 1.95 nN/V. The maximum external normal load range for which the maximum frictional loads, contact areas and pressures measured is shown in Table 2. Using a cantilever with normal spring constant of 0.028 ± 0.003 N/m provided a linear relationship between normal load and the resulting frictional force. The 'μ' determined from the slopes of the best-fit lines (frictional force versus normal load) was 0.22 ± 0.01 (Fig. 5, Table 2).

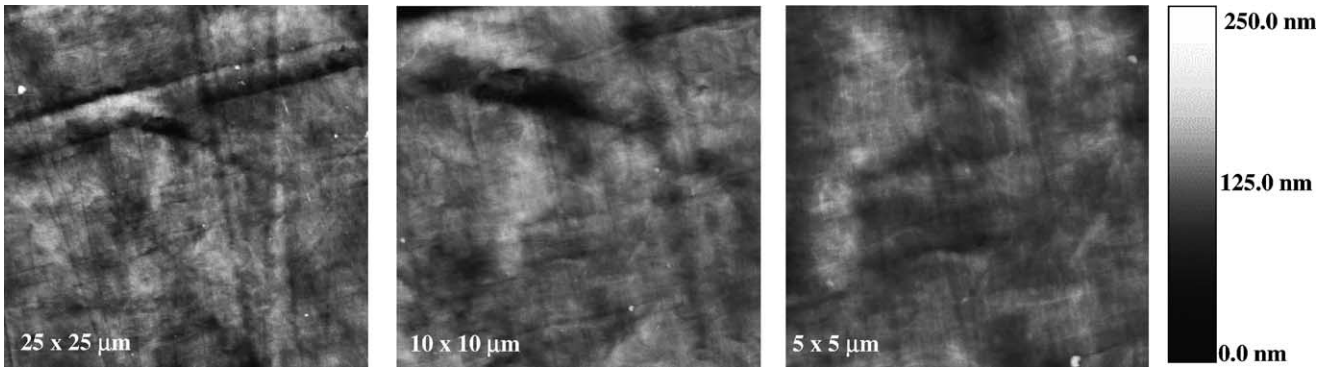

Fig. 4. Atomic force microscopy of direct compression moulded UHMWPE insert of (Maxim^{TM}, Biomet Inc., IN, USA) total knee replacement prosthesis. The surfaces were scanned using a silicon nitride AFM tip, 'V'-shaped, 'D'-type microlever with a normal spring constant of 0.028 ± 0.003 N/m (ThermoMicroscopes, CA, USA).

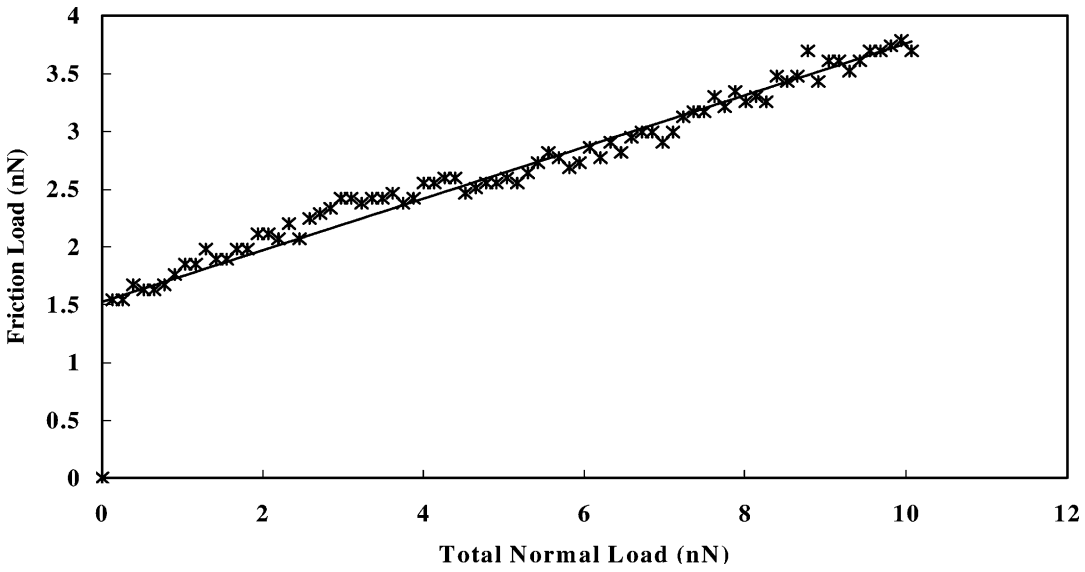

Fig. 5. A representative plot of friction force observed as a function of increase in external normal load for each test using 'D'-type, 'V'-shaped cantilever with a normal spring constant of 0.028 ± 0.003 N/m.

The dependence of frictional load on normal load was non-linear at higher normal loads when the response of the UHMWPE surface was studied using a cantilever with a nominal normal spring constant of 2.1 N/m as shown in Fig. 6. The frictional load was observed to be linear with normal load increase over the three individual regions 'A', 'BC' and 'D'. At certain normal loads given by parameter 'N_{v1}' and 'N_{v2}' (positions B and C), a sudden transition in frictional load was noticed (Fig. 6). The transitions in frictional loads were noticed at approximately the same external normal loads for subsequent tests over different regions on the same sample surface (Fig. 6). An increase in frictional force was observed for the first transient in frictional force at a normal load of 197 ± 9 nN contributing to a maximum contact pressure of 462 ± 9 MPa. The second transient in frictional force was observed at a normal load of 288 ± 13 nN contributing to a maximum contact pressure of 518 ± 13 MPa.

Examination of the surface followed by friction testing using the cantilever with 2.1 N/m spring constant revealed damage on the moulded UHMWPE. The run-in of the hard Si_3N_4 asperity into UHMWPE formed a wear track with UHMWPE material around the wear track. In addition, more material at the leading edge and the trailing edge of the wear track was noticed (Fig. 7). The width and depth of the wear track seen on UHMWPE surface as a result of loading (using a cantilever with a nominal normal spring constant of 2.1 N/m) were 300 nm and 150 nm, respectively.

4. Discussion

When two engineering surfaces come into contact with each other, surface roughness causes an initial contact to occur at discrete regions. The sum of all these areas of discrete contact regions or junctions formed by the asperities

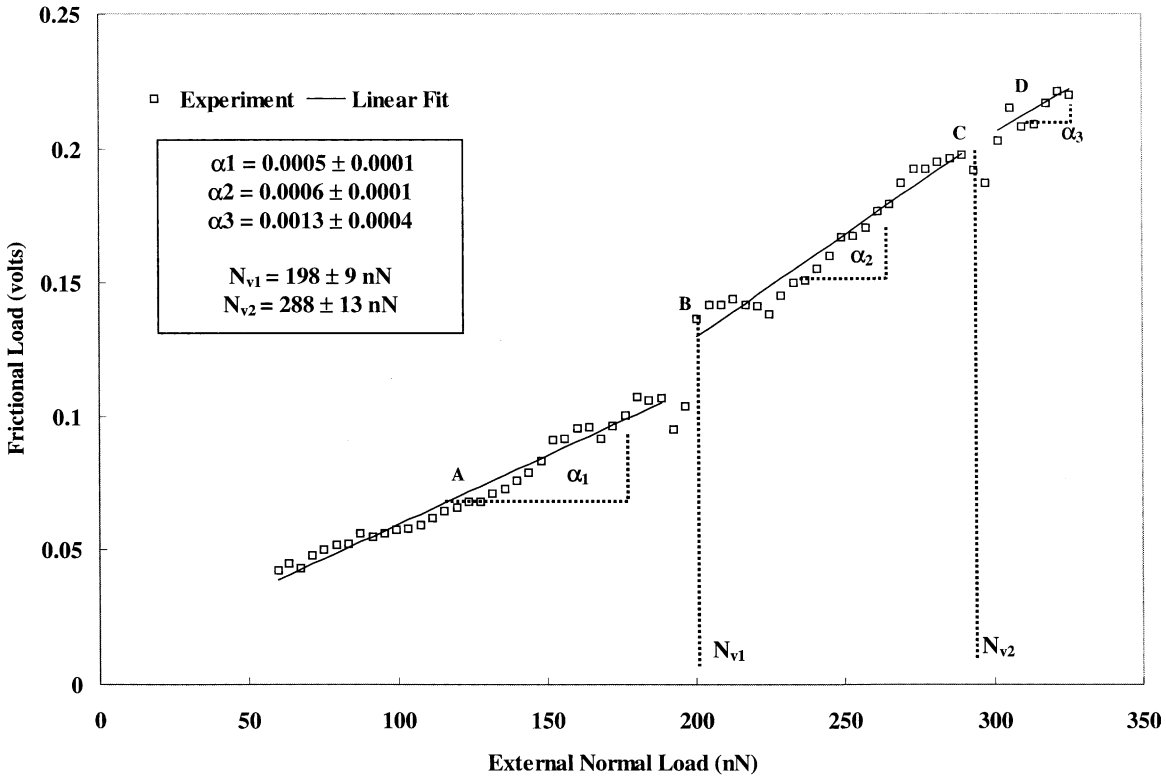

Fig. 6. A representative plot illustrating the observed friction transients as a function of increase in external normal load using 'A'-type, 'V'-shaped cantilever with a nominal spring constant of 2.1 N/m. The average normal load (N_{v1}, N_{v2}) corresponding to a friction transient and average slopes (α_1, α_2, α_3) for three tests ($n = 3$) are specified.

constitutes the real area, which is a small fraction of the apparent area of contact [30]. Abrasive wear is a function of surface roughness, increasing with an increase in surface roughness [30]. The high 'R_a' of the cast CoCr alloy surface (Table 3, Figs. 2 and 3) was indicative of the presence of several peaks. Each peak by itself may be considered as a nanoasperity on the cast CoCr surface sliding against a relatively lower 'R_a' UHMWPE surface, thereby establishing a nanoscale tribocontact within the TJR prosthesis. This study elucidates the frictional characteristics at the interface of one such nanotribocontact by using an AFM as a valid tribosystem to represent the nanocontact in TJR prosthesis. Because the initial contact involves a hard elastic asperity on the cast CoCr alloy surface sliding against a soft compression moulded UHMWPE, the mechanics at the interface of the nanocontact is understood from an elastic–plastic point of view. As stated earlier by others, during contact of elastic–plastic bodies under normal loads, the surface is deformed elastically, with the maximum shear stress occurring, some distance below the center of the contact region [14,15]. The hypothesis of this study was that asperities in the form of hard inclusions on the cast CoCr polished surface sliding on a softer UHMWPE surface under multiaxial loading conditions, damage the interface by plastic deformation of UHMWPE causing abrasive wear, and therefore, generating UHMWPE submicron wear debris.

In this study, BSE and EDX techniques revealed the presence of carbides in cast CoCr alloy components of TJR prosthesis. One of the goals of this study was to define if the Si_3N_4 AFM tip serves as a reasonable nanoscale asperity model for TJR prosthesis. Based on the results, first, a similarity in dimension between the radii of nanoasperities measured on the surface of CoCr and the Si_3N_4 AFM tip was verified, validating the use of the AFM tip as a model asperity in terms of size. Second, Si_3N_4, like the carbide asperity protrusions on the CoCr component polished surface, is a relatively chemically inert ceramic. The interfacial chemistry does not likely play a significant role in the largely mechanical deformation modes observed in this study. Third, the difference in elastic modulus between SiC, Si_3N_4 and CoCr has virtually no effect on the tribological response, since the key parameter governing elastic contact behavior is the combined modulus of the two surfaces, which will be primarily determined by the modulus of UHMWPE. Finally, SiC and Si_3N_4 share similar hardness values (Table 1) and while CoCr is substantially softer than either by a factor of approximately 40, the hardness of UHMWPE is yet two orders of magnitude smaller than that of CoCr. The evolution of plastic deformation will be largely governed by the hardness of the UHMWPE. These facts confirm the use of Si_3N_4 tip as a valid model to represent and simulate asperity nanocontact between

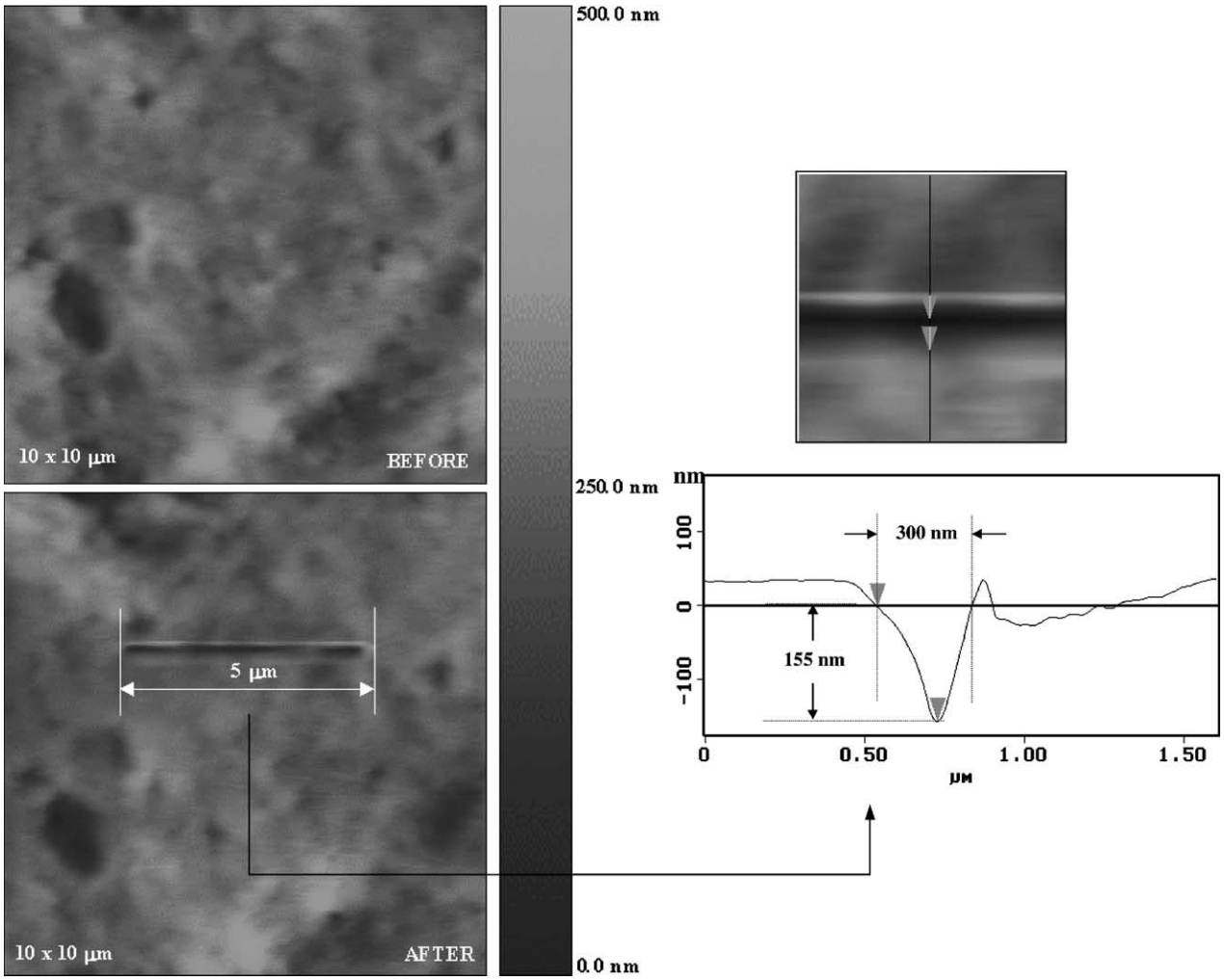

Fig. 7. AFM scans of UHMWPE before and after testing showing ploughing wear track produced at the interface of the tribocontact due to loads placed on the 'A'-type, 'V'-shaped cantilever with a nominal spring constant of 2.1 N/m.

a cast CoCr alloy and UHMWPE components of TJR prostheses.

The evolution of the SiC particles observed on the polished surface of CoCr alloy of TJR prosthesis is two-fold. These particles can arise from the SiC polishing grit particles used for obtaining a mirror finish on the contacting surface of CoCr components and/or carbides within the alloy and its surface in order to increase its wear performance [31]. However, the presence of these particles enables them to act as hard nanoasperities initially establishing a nanocontact with the soft compression moulded UHMWPE (Figs. 2 and 3, Tables 1 and 2) in TJR prosthesis.

The choice of the ranges of normal load and contact area yield different types of interactions between the two contacting surfaces. At low normal loads, elastic forces are dominant and adhesive forces play a significant role. At high normal loads, the hard contacting asperities on the polished surface of CoCr could penetrate the soft UHMWPE possibly causing an abrasive action leading to an increase in the overall friction measurement and a decrease in adhesive forces.

The normal and resulting frictional loads at the nanocontact define the elastic or plastic mechanical response of the softer material. The total normal load range of 1–11 nN caused contact pressures ranging from 14 to 80 MPa which defined the 'μ' of the nanotribocontact in TJR prosthesis to be 0.22 ± 0.01 (Table 2). The steady-state dynamic coefficient of friction at the nanoscale 'μ_{nano}' measured was comparable to the macroscale 'μ_{macro}' when sliding cast CoCr alloy against extruded UHMWPE in dry air [32]. However, at the macroscale, the presence of a lubricant separating the contact between CoCr and UHMWPE decreased the value of 'μ_{macro}' approximately to a minimum of 0.03 and a maximum of 0.11 as was observed by others [33,34]. The low normal loads facilitated in establishing low contact pressures and contact areas, explaining the linearity in reversible energy loss of the material at the interface of the nanocontact in TJR prosthesis (Fig. 5). Because UHMWPE is a semicrystalline material, the reversible mechanical response at each externally placed normal load could be caused by amorphous and crystalline phases over a scan length of 1 μm. However,

it should be understood that if the frictional response of the material for every increment in normal load over the same region of sliding is not acquired within the fatigue limit of UHMWPE, then it is likely that one may capture a transition in frictional response. This is due to the failure of the UHMWPE caused by repeated sliding of the harder asperity of cast CoCr alloy which, is explained below.

At some critical normal load, the combination of normal and resulting shear loads (multiaxial loading) exceed the yield strength of UHMWPE causing permanent deformation. The use of a cantilever with a higher nominal spring constant of 2.1 N/m compared to 0.03 N/m accelerated the initiation of permanent or irreversible damage at the interface of the nanocontact. The choice of a stiffer cantilever facilitated in applying normal loads ranging from 17 to 340 nN with a contact pressure corresponding to 209–552 MPa (Table 2).

From Fig. 6, below a normal load of 200 nN (region 'A'), a steady linear behavior of frictional load was observed. It could be argued that within this region, the deformation of UHMWPE, as was noticed using the lateral force mode of Nanoscope E, was predominantly within the elastic limit once again justifying that the reversible energy loss was the contributing factor to the measured 'μ' of TJR prosthesis. A similar normal load was observed by Niederberger et al. [17], when testing high density polyethylene and low density polyethylene under loading conditions specified as above. As the normal load was increased, the contact pressure increased until the plastic zone in the subsurface reached the surface and began to embrace the counterpart (point 'B'). The deformation in the material caused an increase in contact area corresponding to an increase in angular twist of the cantilever explaining the observed sudden jump at point 'B' and the significant increase in slope of region 'BC' over region 'A' (Fig. 6).

The sudden jump in friction at 'B' (Fig. 6) and the significant increase in slope of regions 'BC' over 'A' could be explained in terms of strain softening of the polymer [7] occurring upon application of shear load at an ambient temperature which is above the glass transition temperature of UHMWPE ($T_g \sim -120\,^{\circ}C$) [35]. Strain softening can occur due to deformation of the amorphous phase on the UHMWPE surface before deformation in crystalline lamellae is observed, or could be a combination of deformations observed within both phases or between the two phases of the polymer. This transition seen in frictional force at a certain normal load can be associated with molecular movement of polymeric chains due to elastic deformation, slip, kinking, melting, twinning, recrystallization or phase transition thus realigning the nanostructure and redefining its physical and mechanical properties resulting in an altered frictional response as explained by others [17,36–39]. The UHMWPE region in contact with the nanoasperity changes from elastic to elastic plastic followed by plastic behavior, which is defined by region 'BC'. At point 'C' the drop in friction could be associated with removal of the material from the run-in or break-in sliding region followed by a steady linear frictional load increase for an increase in external normal load defined by region 'D'.

State-of-the-art polishing techniques are used for the surgical grade CoCr components that are used in TJR prosthesis. It has been shown that the resulting surface finish, which contains scratches of quantifiable widths and depths, affects the wear performance of the implant. However, retrieved implants from patients were found to have numerous scratches of greater width and depth than those created during manufacturing [7]. Such scratches have also been achieved in simulations. In these simulations, permanent deformation normally occurs at the tips of intimate asperity contacts within the softer material [14,18]. This irreversible phenomenon can occur at each of these contact regions. From a macroscopic point of view, plastic strain is built into each contact causing the material to flow. Upon repeated sliding, this large-scale irreversible deformation leads to the loosening of wear particles at the nanotribocontact of the material.

In this work, the run-in of the harder asperity into the surface of the softer component was understood by the process of plastic deformation and by ploughing of the harder asperity into the softer material. The plastic flow of the material causes the formation of a wedge-shaped grooved by displacing the polymeric material from the center of the loading path to the sides (Fig. 7). Accumulation of this material over repeated cycles could eventually detach and cause the formation of loose submicron wear particles in TJR prosthesis.

The presence of carbides in the polished surface of a femoral component and the frictional response of UHMWPE at the interface of the nanotribocontact can lead to surface abrasion from protruding hard carbides that exist within the cast CoCr alloy of TJR prosthesis. In addition, it can be stated that the plastic deformation of the material under multiaxial loading conditions (normal and resulting shear) during sliding can be used to explain the initiation of failure of the polymeric material in TJR prosthesis eventually leading to submicron UHMWPE particle generation.

5. Conclusions

This study demonstrated the frictional characteristics at the nanointerface of TJR prosthesis by using an AFM as a valid tribosystem. A similarity in dimension and mechanical properties between SiC nanoasperities measured on the surface of CoCr and Si_3N_4 AFM tip allows the use of a contact mode AFM as a test bed to represent and simulate asperity nanocontact between a cast CoCr alloy and UHMWPE components of TJR prosthesis. The evolution of the silicon carbide particles observed on the polished surface of CoCr alloy of TJR prosthesis can arise from the SiC polishing grit particles and/or carbides within the alloy and its surface in order to increase its wear performance. However, the presence of these particles enables them to act as hard nanoasperities initially establishing a nanocontact with the soft compression moulded UHMWPE.

The evolution of large-scale irreversible deformations also defined as plastic deformation could lead to ultimate failure of the material at the nanotribocontact upon repeated sliding and ploughing. The run-in of the harder asperity into the surface of the softer component was understood by defining plastic deformation of material followed by a groove formation eventually leading to the formation of a wedge around the groove. Accumulation of this material over repeated cycles could eventually detach and cause the formation of loose submicron wear particles in TJR prosthesis.

Acknowledgements

This work was supported by the National Science Foundation (EPS 9871943) and Fullerton Foundation. The authors thank Biomet Inc. (IN, USA) for the use of CoCr and UHMWPE total knee replacement prosthesis. In addition, the authors thank Joan Hudson, Electron Microscopy Laboratory, Clemson University, Clemson, SC, for her expertise in energy dispersive X-ray analysis and back scattering energy techniques. Dr. Larry Grimes, Department of Statistics, Clemson University, SC is greatly acknowledged for the statistical analysis expertise. The authors thank Ms. Laura Riester for nanoindentation experiments and her technical expertise. Nanoindentation research was sponsored by the Assistant Secretary for Energy Efficiency and Renewable Energy, Office of Transportation Technologies, as part of the High Temperature Materials Laboratory User Program, Oak Ridge National Laboratory, managed by UT-Battelle, LLC, for the US Department of Energy under contract number DE-AC05-00OR22725.

References

[1] S. Li, A.H. Burstein, J. Bone Joint Surg. 76-A (7) (1994) 1080–1090.
[2] S.M. Kurtz, O.K. Muratoglu, M. Evans, A.A. Edidin, Biomaterials 20 (1999) 1659–1688.
[3] K.R.S. John, R.A. Poggie, L.D. Zardiackas, R.M. Afflitto, in: J.A. Disegi, R.L. Kennedy, R. Pilliar (Eds.), Cobalt-Base Alloys for Biomedical Applications, ASTM-STP 1365, American Standards for Testing Materials, West Conshohocken, PA, 1999, pp. 145–155.
[4] C. Klapperich, K. Komvopolous, L. Pruitt, J. Tribol-T. ASME 121 (2) (1999) 394–402.
[5] G. Lewis, J. Biomed. Mater. Res. (Appl. Biomater.) 38 (1997) 55–75.
[6] S.P. Ho, P.F. Joseph, M.J. Drews, M. LaBerge, in: Proceedings of the Transactions of the 28th Annual Meeting Society for Biomaterials, Tampa, Florida, 23–27 April 2002.
[7] A. Wang, B. Edwards, S. Yau, V.K. Polineni, A. Essner, R. Klein, D.C. Sun, C. Stark, J.H. Dumbleton, in: R.A. Gsell, H.L. Stein, J.J. Ploskonlea (Eds.), Characterization and Properties of UHMWPE, ASTM STP 1307, American Standards for Testing Materials, West Conschohocken, PA, 1998, pp. 56–76.
[8] J. Fisher, J. Bell, P.S.M. Barbour, J.L. Tipper, J.B. Matthews, A.A. Besong, M.H. Stone, E. Ingham, J. Eng. Med. 215 (H2) (2001) 127–132.
[9] A. Wang, A. Essner, R. Klein, J. Eng. Med. 215 (H2) (2001) 133–139.
[10] D.L. Bartel, J.J. Rawlinson, A.H. Burstein, C.S. Ranawat, W.F. Flynn, Clin. Orthop. 317 (1995) 76–82.
[11] R.J. Jacob, D. Pienkowski, D.P. Hoglin, K.A. Saum, H. Kaufer, P.J. Nicholls, J. Biomed. Mater. Res. 37 (4) (1997) 489–496.
[12] D. Pienkowski, D.P. Hoglin, R.J. Jacob, K.A. Saum, P.J. Nicholls, H. Kaufer, J. Biomed. Mater. Res. 33 (2) (1996) 65–71.
[13] N.K. Myshkin, M.I. Petrokovets, S.A. Chizhik, Tribol. Int. 31 (1-3) (1998) 79–86.
[14] F.P. Bowden, D. Tabor, Friction—An Introduction to Tribology, Anchor Press/Doubleday, New York, 1973, pp. 54–55, p. 65.
[15] N.P. Suh, Tribophysics, Prentice-Hall, New Jersey, 1986, pp. 128–129.
[16] J. Hu, X. Xiao-D, F.D. Ogeltree, M. Salmeron, Surf. Sci. 327 (1995) 358–370.
[17] S. Niederberger, D.H. Gracias, K. Komvopoulous, G.A. Somorjai, J. Appl. Phys. 87 (6) (2000) 3143–3150.
[18] R.W. Carpick, M. Salmeron, Chem. Rev. 97 (1997) 1163–1194.
[19] H. Hampel, L.G. Hector, N.T. Nuhfer, H.R. Piehler, in: Proceedings of the Transactions of the 44th Annual Meeting of the Orthopaedic Research Society, New Orleans, Louisiana, 16–19 March 1998, 365 pp.
[20] S.R. Schmid, L.G. Hector, J. Elings, H. Hampel, H. Piehler, Fundamentals of nanoindentation and nanotribology, in: N.R. Moody, W.W. Gerberich, N. Burham, S.P. Baker (Eds.), Proc. Mater. Res. Soc. Symp. 522 (1998) 391–397.
[21] S.M. Kurtz, L. Pruitt, C.W. Jewett, R.P. Crawford, D.J. Crane, A.A. Edidin, Biomaterials 19 (1998) 1989–2003.
[22] S.A. Rowland, S.W. Shalaby, R.W. Latour, A.F. von Recum, J. Appl. Biomater. 6 (1) (1995) 1–7.
[23] S.P. Ho, L. Riester, M. Drews, T. Boland, M. LaBerge, J. Eng. Med. 216 (H) (2002) 123–133.
[24] M.F. Doerner, W.D. Nix, J. Mater. Res. 1 (1986) 601–609.
[25] W.C. Oliver, G.M. Pharr, J. Mater. Res. 7 (6) (1992) 1564–1583.
[26] F.D. Ogeltree, W.R. Carpick, M. Salmeron, Rev. Sci. Instrum. 67 (9) (1996) 3298–3306.
[27] J.L. Hutter, J. Bechhoefer, Rev. Sci. Instrum. 64 (7) (1993) 1868–1873.
[28] K.L. Johnson, K. Kendall, A.D. Roberts, Proc. R. Soc. Lond. A 324 (1971) 301.
[29] J. Neter, W. Wesserman, M.H. Kutner, Applied Linear Statistical Models, 2nd ed., Irwin (Richard D.), Homewood, IL, 1985, 349 pp.
[30] B. Bhushan, Principles and Applications of Tribology, Wiley, New York, 1999, 553 pp.
[31] A. Wang, J.D. Bobyn, S. Yue, J.B. Medley, F.W. Chan, in: J.A. Disegi, R.L. Kennedy, R. Pilliar (Eds.), Cobalt-Base Alloys for Biomedical Applications, ASTM-STP 1365, American Society for Testing Materials, West Conshohocken, PA, 1999, pp. 125–134.
[32] P. Huang, A. Salinas-Rodriguez, H.F. Lopez, Mater. Sci. Technol. 15 (1999) 1324–1330.
[33] H.A. McKellop, I.C. Clarke, K.L. Markolf, H. Amstutz, J. Biomed. Mater. Res. 12 (1978) 895–927.
[34] M. Ungethum, H.J. Refior, Archiv fur Orthopadische and Unfall-Chirurgie 79 (1974) 97.
[35] S.L. Agrawal, Physical constants of polyethylene, in: J. Brandup, E.H. Immergut (Eds.), Polymer Handbook, Wiley, New York, 1975, V-13 p.
[36] R.W. Meyer, L.A. Pruitt, Polymer 42 (2001) 5293–5306.
[37] B. Wunderlich, Macromolecular physics, vol. 1, Crystal Structure, Morphology, Defects, Academic Press, New York/London, 1973, pp. 489–499.
[38] S.G. Truley, H.A. Keskkula, J. Polym. Sci.: Part C 14 (1966) 69–87.
[39] P. Predecki, A.W. Thornton, J. Appl. Phys. 41 (1970) 4342.